Parallel Operation of Bidirectional Interfacing Converters in a Hybrid AC/DC Microgrid Under Unbalanced Grid Voltage Conditions

Kai Sun, *Senior Member, IEEE*, Xiaosheng Wang, *Student Member, IEEE*, Yun Wei Li, *Senior Member, IEEE*, Farzam Nejabatkhah, *Student Member, IEEE*, Yang Mei, *Member, IEEE*, and Xiaonan Lu, *Member, IEEE*

***Abstract*—Today, interests on hybrid ac/dc microgrids, which contain the advantages of both ac and dc microgrids, are growing rapidly. In the hybrid ac/dc microgrid, the parallel-operated ac/dc bidirectional interfacing converters (IFCs) are increasingly used for large capacity renewable energy sources or as the interlinking converters between the ac and dc subsystems. When unbalanced grid faults occur, the active power transferred by the parallel-operated IFCs must be kept constant and oscillation-free to stabilize the dc bus voltage. However, under conventional control strategies in unbalanced grid conditions, the active power transfer capability of IFCs is affected due to the converters' current rating limitations. Moreover, unbalanced voltage adverse effects on IFCs (such as output power oscillations, dc-link ripples, and output current enhancement) could be amplified by the number of parallel converters. Therefore, this paper investigates parallel operation of IFCs in hybrid ac/dc microgrids under unbalanced ac grid conditions and proposes a novel control strategy to enhance the active power transfer capability with zero active power oscillation. The proposed control strategy employs a new current sharing method which introduces adjustable current reference coefficients for parallel IFCs. In the proposed control strategy, only one IFC, named as redundant IFC, needs to be designed and installed with higher current rating to ensure the constant and oscillation-free output active power of parallel IFCs. Simulation and experimental results verify the feasibility and effectiveness of the proposed control strategy.**

***Index Terms*—Bidirectional interfacing converter, hybrid ac/dc microgrid, parallel converters, unbalanced grid voltages.**

I. Introduction

In recent years, due to the integration of dc power sources such as fuel cells, photovoltaic (PV) panels, and storage elements (SEs) along with modern dc loads in microgrids, and considering the existence of century-long ac power systems, interests in hybrid ac/dc microgrids are growing rapidly. The ac/dc microgrids contain distributed generation (DG) units and loads connected to both ac and dc subsystems [1]–[3]. In hybrid ac/dc microgrids, interfacing converter (IFC) is the critical link between ac and dc buses/subsystems. These IFCs are used in parallel when larger power and current capacity is needed. These parallel converters can be the interlinking converters between ac and dc subsystems (parallel solid-state transformers). Moreover, DGs/SEs with large capacity can also be connected to the ac subsystem through parallel IFCs.

In early studies, the load power sharing among parallel converters was investigated in ac and dc microgrids. Various control methods have been proposed such as centralized control [4], master–slave control [5], and droop control [6]–[8] to share the output power in proportion to the power rating of each converter. However, the control of IFCs in hybrid ac/dc microgrids is more challenging. In recent years, studies on parallel IFCs' control in hybrid ac/dc microgrids have been done in the literature [9]–[12]. A coordinate control method for the hybrid microgrid is proposed in [9], and a generalized droop control method is proposed to achieve the proper power sharing in a hybrid microgrid in [11]. Hierarchical control of IFCs in hybrid microgrids is proposed in [12] as a means of restoring voltage deviations produced by the droop control and facilitating proper power exchange between the microgrid and the utility grid. In this method, different operation modes of a hybrid microgrid are investigated, and the IFCs act as either inverters or rectifiers.

However, the presence of unbalanced faults in the ac utility grid affects the operation of grid-connected converters, especially IFCs [13], [14]. For IFCs under grid faults, active power and reactive power oscillations are important problems, which may result in dc-link oscillation and instability. Also, overcurrent might occur when grid voltage becomes unbalanced, which restrict power transfer capability of IFCs. Beside, voltage and current distortion would occur if the control strategy is not properly designed. To solve these problems, efforts have been done to develop control schemes of IFCs in the presence of unbalanced grid faults [13]–[24]. These control strategies are mainly based on the symmetrical component analysis and can be divided into three categories according to their control targets. The first group of control strategies focuses on instantaneous active power control, and some researchers have solved the problem of dc-link ripple by eliminating active power oscillation [15]–[17]. The

Manuscript received September 15, 2015; accepted March 10, 2016. Date of publication April 20, 2016; date of current version December 9, 2016. This work was supported by the National High Technology Research and Development Program (863 Program, 2015AA050606), by the National International Science and Technology Cooperation Project 2014DFG62610, by the National Natural Science Foundation of China under Grant 51177083, and by the State Key Lab of Power Systems under Grant SKLD14M01 in Tsinghua University, China. Recommended for publication by Associate Editor J. A. Pomilio.

K. Sun and X. Wang are with the State Key Lab of Power Systems, Department of Electrical Engineering, Tsinghua University, Beijing 100084, China (e-mail: sun-kai@mail.tsinghua.edu.cn; wangxs07@163.com).

Y. W. Li and F. Nejabatkhah are with the Department of Electrical and Computer Engineering, University of Alberta, Edmonton, AB T6G 2R3 Canada (e-mail: yunwei.li@ualberta.ca; nejabatk@ualberta.ca).

Y. Mei is with the College of Electrical and Control Engineering, North China University of Technology, Beijing 100144, China (e-mail: meiy@ncut.edu.cn).

X. Lu is with Energy Systems Division, Argonne National Laboratory, Lemont, IL 60439 USA (e-mail: xiaonan.charles.lu@gmail.com).

Color versions of one or more of the figures in this paper are available online at http://ieeexplore.ieee.org

Digital Object Identifier 10.1109/TPEL.2016.2555140

second group of control strategies focuses on the power quality at the point of common coupling (PCC), and the DG converter works as a compensator and supports the grid voltage [18]–[20]. For instance, by controlling the negative-sequence conductance of DG inverters, negative-sequence voltages at PCC can be eliminated in [18]. Reactive power is injected into the grid to prevent undervoltage in the faulted phases and overvoltage in the nonfaulted phases in [19], which renders the DG units more capable of ride-through. The third type of control strategies involves both controllable active and reactive power oscillations at the same time and the peak current limitation and the current THD [21]–[25]. For example, in [24], a continuous-adjustable coefficient is proposed in which amplitude of active and reactive powers oscillations can be adjusted continuously on the premise of sinusoidal output currents. Different control objectives can be achieved in various application scenarios.

However, studies on the control of parallel IFCs under unbalanced grid voltage conditions are quite limited. During the parallel operation of IFCs, the active power oscillation under unbalanced grid voltage could be amplified by the number of parallel converters and is one of the main concerns due to its impact on dc-link voltage. For this reason, the active power oscillation of parallel IFCs should be controlled during grid fault events. For single IFC, if the oscillation-free and constant output power under unbalanced grid faults is desired, the three-phase currents of the IFC would be unbalanced and the peak current would increase to ensure the constant active power. In this case, the peak current may exceed the converter current rating limit. To avoid this problem, the reference power of converter should be reduced. As a result, in a single IFC, the oscillation-free output power may cause the reduction of active power transfer capability. For parallel IFCs, this would significantly reduce the power transfer capability between ac and dc buses under grid faults. One solution is to use converters with higher current ratings, which is not cost effective. Thus, it is desirable to propose a new control scheme to keep the power transfer capability constant without increasing the current rating of all IFCs.

The authors have proposed a novel control strategy for parallel-operated bidirectional IFCs in hybrid ac/dc microgrids under unbalanced ac grid voltage conditions in [26], in which the key idea and implementation of this control strategy have been presented. However, the complete design considerations, experimental verification, and analysis have not been involved. Hence, this paper is an extension of [26]. The proposed control strategy introduces adjustable current reference coefficients for parallel IFCs in order to enhance the active power transfer capability with zero active power oscillation. In the proposed control strategy, only one IFC, called as redundant IFC, needs to have higher current rating in comparison to other IFCs. This paper is organized as follows. Section II shows how the current rating of converters limits active power transfer capability. Section III describes the proposed two-level regulation scheme for parallel IFCs in detail. Control system design is also introduced and discussed. Section IV provides the simulation results and analysis of the two-level regulation scheme. Experimental verifications are provided in Section V. Section VI summarizes the paper and lists conclusion.

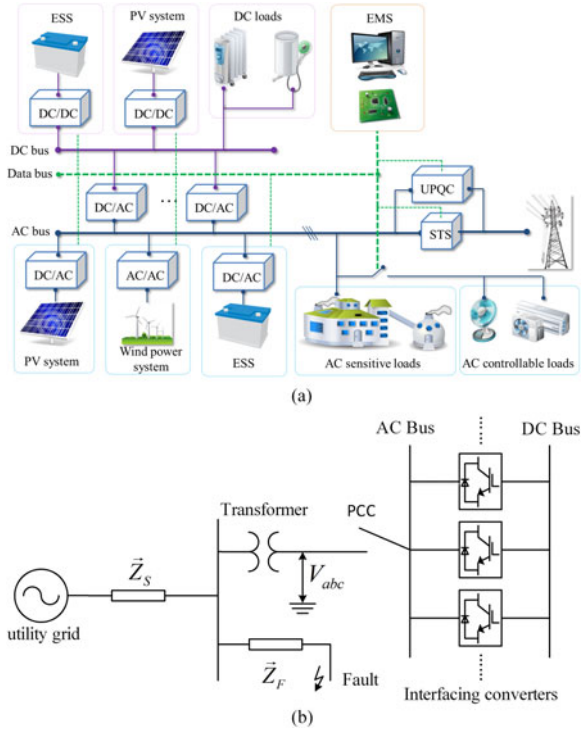

Fig. 1. (a) Hybrid ac/dc microgrid with parallel IFCs. (b) Parallel IFCs connection to the utility grid.

II. Parallel IFCs Active Power Transfer Capability

Fig. 1(a) shows a typical hybrid ac/dc microgrid with parallel IFCs between ac and dc subsystem. The ac subsystem is connected to the utility grid through transformers at PCC. In this microgrid, energy storage system, PV system, wind power system, and different ac/dc loads are connected to ac or dc buses directly or through corresponding IFCs. In most cases, energy management system (EMS) is necessary to realize control of the whole system. Active power reference value is sent from EMS to each IFC through data bus. In this system, digital signal processors (DSPs) are needed for each IFC. For parallel IFCs, a master–slave communication structure is utilized. One IFC is configured as master converter and others are slave converters. Some critical control parameters could be sent from master to slave through data bus. A typical connection between parallel IFCs and the utility grid is presented in Fig. 1(b), where a grid fault is considered as a source of unbalance.

In this paper, IFCs under unity power factor operation are considered. That is to say, average reactive power of IFCs is zero and only active power transfer is considered. Actually, in some situations, it is also desired to transfer average reactive power between ac and dc buses. Reactive power transfer is not involved in this paper. Considering symmetric-sequence-based instantaneous power theory, the output active and reactive power of each IFC is calculated as follows [24]:

$$\begin{aligned} p &= \underbrace{\left(v^+ \cdot i_p^+ + v^- \cdot i_p^-\right)}_{P} + \underbrace{\left(v^+ \cdot i_p^- + v^- \cdot i_p^+\right)}_{\Delta P} \\ q &= \underbrace{v_\perp^- \cdot i_p^+ + v_\perp^+ \cdot i_p^-}_{\Delta Q}. \end{aligned} \tag{1}$$

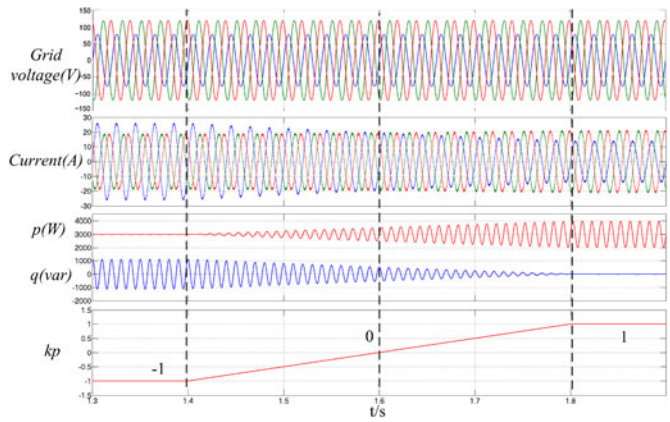

Fig. 2. Simulation waveforms of an IFC under different k_p values.

Here, P and ΔP are the average and oscillatory terms of instantaneous active power, and v^+ and v^- are the positive- and negative-sequence vectors of grid voltages, respectively. Here, i_p^+ and i_p^- are positive- and negative-sequence currents, respectively. In this paper, current reference algorithm proposed in [24] is taken as an example to illustrate the control strategy of parallel IFCs under grid fault. By assuming that the two terms of the active power oscillations counteract each other, a current reference coefficient k_P can be defined as follows:

$$v^+ \cdot i_p^- = -k_p v^- \cdot i_p^+, \quad 0 \le k_p \le 1. \tag{2}$$

After some manipulation, the current reference of IFC can be determined as in (3), where k_P is an adjustable coefficient

$$i_p^* = \frac{P}{\|v^+\|^2 + k_p\|v^-\|^2} v^+ + \frac{k_p P}{\|v^+\|^2 + k_p\|v^-\|^2} v^-, \quad -1 < k_p < 1. \tag{3}$$

Here, P is the reference active power and i_p^* is the current reference of IFC. From (1) and (3), the instantaneous active and reactive powers can be calculated as follows:

$$p = P + \frac{P(1+k_p)(v^- \cdot v^+)}{\|v^+\|^2 + k_p\|v^-\|^2}, \quad q = \frac{P(1-k_p)(v_\perp^- \cdot v^+)}{\|v^+\|^2 + k_p\|v^-\|^2}. \tag{4}$$

Considering (4), it can be understood that active and reactive powers can be controlled using k_p. In order to study the influence of k_p on the oscillation of active and reactive powers, a single grid-connected IFC under unbalanced grid faults has been simulated as a case study in Fig. 2. The grid fault is a two-phase to ground fault, as shown in Fig. 1(b), and it is assumed that $\overrightarrow{Z}_s = \overrightarrow{Z}_f$. If the transformer in Fig. 1(b) is a $\Delta - Y$ transformer, the voltage fault will change to type F fault at PCC after propagation [27]. Positive- and negative-sequence components of fault voltage are 2/3 and 1/6 of the nominal value. Phase angle difference of positive- and negative-sequence components is 180°. The utility grid is three-phase 110 Vrms/ 50 Hz. Active power reference is 3000 W and reactive power reference is zero. In Fig. 2 at the top, three-phase voltage waveforms are shown. As clear from the figure, active and reactive powers are free from oscillations when $k_P = -1$ and $k_p = 1$, respectively, which can be verified by (4). Moreover, the three-phase currents are balanced when $k_P = 0$ [see (3)]. As shown in this figure, the output currents of each IFC are highly unbalanced under zero active power oscillation. Since this unbalanced current may exceed IFC current rating limit, the output active power reference must be reduced. As a result, in order to keep the output active power at constant and oscillation-free value, the corresponding control strategy of parallel IFCs is proposed.

Here, current reference of [24] is taken as an example to verify the proposed control strategy in our paper. Indeed, other current reference algorithm could also be used for IFCs under unbalanced grid faults. For example, Castilla *et al.* [21], [22] have proposed another control scheme with adjustable power quality characteristics using coefficients α and β. Using this algorithm, we could also get the proposed control strategy to enhance active power transfer capability of IFCs under grid faults.

If not specified, the grid fault is considered as a type F fault as in Fig. 2. However, according to the following theoretical analysis, the proposed control strategy is applicable in all kinds of unbalanced grid faults. Besides, the control strategy could also work under balanced grid fault, which might also occur in utility grid.

A. Power Complementary Strategy: Oscillation-Free Active Power Transfer of Parallel IFCs

Considering aforementioned discussions, the oscillation-free active power transfer can be facilitated under $k_p = -1$ in all IFCs. However, because the IFCs peak current may exceed the current rating limits, the converters may not be able to transfer as much active power as under normal grid voltage conditions. Therefore, following control scheme is proposed to transfer constant and oscillation-free active power of parallel IFCs. In this scheme, the active power transferred by each IFC can oscillate, but they complement each other in parallel form to cancel out power oscillations.

Considering two parallel IFCs, the collective active power oscillation can be calculated as follows:

$$\Delta P_A + \Delta P_B = P(v^- \cdot v^+)\left(\frac{1+k_A}{\|v^+\|^2} + k_A\|v^-\|^2 + \frac{1+k_B}{\|v^+\|^2 + k_B\|v^-\|^2}\right). \tag{5}$$

k_A and k_B are coefficient k_p of converters A and B, respectively. Considering (5), in order to ensure oscillation-free active power transferring and constant dc bus voltage, it is required that $\Delta P_A + \Delta P_B = 0$. Assuming $\|v^+\|^2 = a$ and $\|v^-\|^2 = b$, the following constraint for active power oscillations cancellation in two parallel IFCs can be determined (see Appendix A)

$$\frac{1}{a + b \cdot k_A} + \frac{1}{a + b \cdot k_B} = \frac{2}{a - b}. \tag{6}$$

Considering (5) and (6), the total transferred active power of two parallel IFCs can be constant without oscillation even though the active power of each converter is oscillating. In (6),

$k_A = k_B = -1$ is the only particular solution. This constraint can be extended to *n* parallel IFCs as follows:

$$\sum_{i=1}^{n} \frac{1}{a + b \cdot k_i} = \frac{n}{a - b}. \tag{7}$$

Considering (7), the collective active power of *n* parallel converters will be oscillation-free if (7) is satisfied. Similarly, total reactive power oscillation of two converters can be calculated if (6) is satisfied (see Appendix B). For *n* converters in parallel, if (7) is satisfied, the reactive power oscillation of *n* parallel IFCs can be obtained as follows:

$$\sum_{i=1}^{n} \Delta Q_i = \frac{2nP(v_{\perp}^{-} \cdot v^{+})}{\|v^{+}\|^2 - \|v^{-}\|^2}. \tag{8}$$

As shown in (8), the reactive power oscillation of parallel IFCs is not affected by k_p, and it only depends on the reference active power and the positive- and negative-sequence grid voltages. As long as (7) is satisfied, the reactive power oscillation remains constant.

However, the variation of k_p of a converter would result in the variation of its peak current value. Considering aforementioned discussions, the adjustable coefficients enable the regulation of peak currents in parallel IFCs and ensure the oscillation-free active power transformation of parallel IFCs at the same time.

B. Influence of Adjustable Coefficients k_p on the Peak Currents of IFCs

Since the peak currents of IFCs may exceed their current rating limits under unbalanced grid faults, the active power transfer capability of IFCs is restricted. Therefore, it is necessary to calculate the peak currents under unbalanced grid faults and investigate the influence of k_p on them. As shown in (3), the current reference of each IFC can be rewrite as follows [27]:

$$\begin{aligned} i_p^* &= \frac{P}{\|v^{+}\|^2 + k_p\|v^{-}\|^2} v^{+} + \frac{k_p P}{\|v^{+}\|^2 + k_p\|v^{-}\|^2} v^{-} \\ &= C_1 v^{+} + C_2 v^{-} = i_p^{+} + i_p^{-}, \quad -1 < k_p < 1. \end{aligned} \tag{9}$$

Here, $v^{+} = V^{+} e^{j(\omega t + \varphi^{+})}$ and $v^{-} = V^{-} e^{j(-\omega t - \varphi^{-})}$. Fig. 3 shows the locus of the grid voltage and the current reference in which θ is defined as $\theta = (\varphi^{+} - \varphi^{-})/2$ $(k_p > 0)$ or $\theta = \pi/2 + (\varphi^{+} - \varphi^{-})/2$ $(k_p < 0)$. The large and small dashed circles are the loci of positive- and negative-sequence current references, respectively. The locus of the total current reference is an ellipse, which has a semimajor axis and semiminor axis. The lengths of the semimajor axis and the semiminor axis are $I_L = |C_1|\|v^{+}\| + |C_2|\|v^{-}\|$ and $I_S = |C_1|\|v^{+}\| - |C_2|\|v^{-}\|$. As shown in Fig. 3, the current reference can be expressed as

$$i_p = \begin{bmatrix} i_\alpha \\ i_\beta \end{bmatrix} = \begin{bmatrix} I_L \cos(\omega t) \\ I_S \sin(\omega t) \end{bmatrix}. \tag{10}$$

As shown in Fig. 3, the peak current at each phase is the maximum projection of the current ellipse on the *abc*-axis. As shown in (10) and Fig. 3, the current reference components on the *abc*-axis can be obtained as follows:

$$i_x' = I_L \cos\gamma \cdot \cos(\omega t) - I_S \sin\gamma \cdot \sin(\omega t), \quad x = a, b, c \tag{11}$$

Here, γ, the rotation angle, is equal to θ, $\theta + \pi/3$, and $\theta - \pi/3$ for the *abc*-axis. Using (11), the maximum current at each phase and the maximum current of IFC under unbalanced grid faults can be expressed as follows:

$$\begin{aligned} I_x^{\max} &= \sqrt{(I_L \cos\gamma)^2 + (I_S \sin\gamma)^2}, \quad x = a, b, c \\ &\Rightarrow I_{\max} = \max(I_a^{\max}, I_b^{\max}, I_c^{\max}). \end{aligned} \tag{12}$$

Considering (12), the peak current of each IFC under unbalanced grid fault conditions depends on the amplitude and phase angle of the grid voltage, the reference power, and the adjustable coefficient k_p. Fig. 4 gives the relationship between the grid fault voltage and the peak current of IFC. The grid condition is the same as that in Fig. 2. The left part shows the peak current when the phase angle difference varies from 0° to 360°. Here, the phase angle difference is defined as $\varphi^{+} + \varphi^{-}$ in Fig. 3. The peak current related to the phase angle is periodic waveform with a period of 120°. In Fig. 4, $k_p = 1$ and $k_p = -1$ are taken as examples to show the relationship. Actually, when $k_p > 0$, the relationship is similar to that when $k_p = 1$, while it is similar to $k_p = -1$ when $k_p < 0$. When $k_p < 0$, peak current reaches its maximum value at 60°, 180°, and 300°, while it reaches its minimum value at 120° and 240°. When $k_p > 0$, peak current reaches its maximum value at 120° and 240°, while it reaches its minimum value at 60°, 180°, and 300°. The right part of Fig. 4 shows how peak current varies with the ratio of negative-sequence voltage to positive-sequence voltage. The peak current rises with higher ratios of negative-sequence voltage. Here, $k_p = 1$ and $k_p = -1$ are taken as examples to show the relationship. Actually, when $k_p > 0$, the relationship is similar to that when $k_p = 1$, while it is similar to $k_p = -1$ when $k_p < 0$. When $k_p < 0$, peak current rises dramatically as

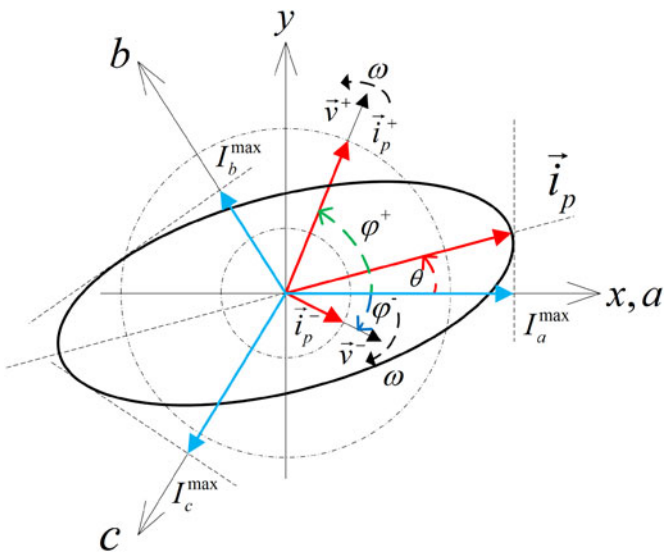

Fig. 3. Locus of the peak currents of IFCs under unbalanced grid faults.

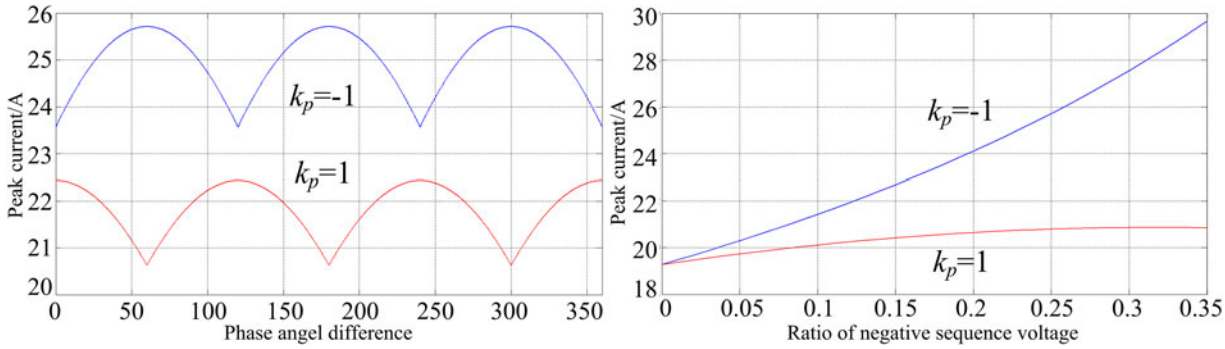

Fig. 4. Influence of the fault voltages on peak currents.

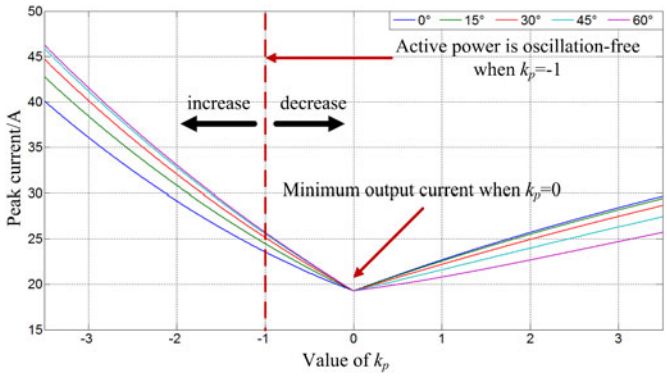

Fig. 5. Peak currents of IFC with adjustable coefficients.

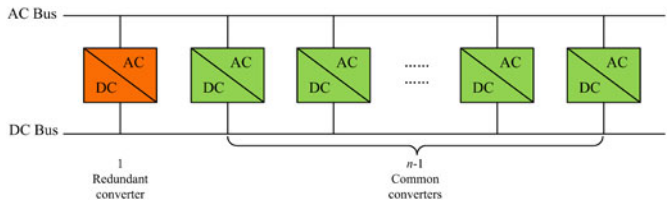

Fig. 6. Parallel IFCs with one redundant converter.

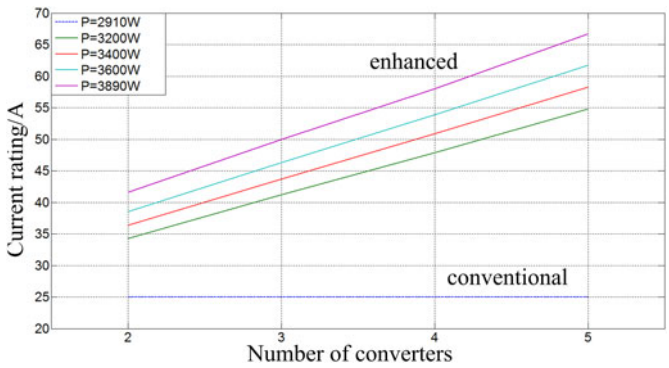

Fig. 7. Current rating of the redundant converter.

ratio of negative-sequence voltage increases. When $k_p > 0$, however, peak current rises slowly and becomes saturated as ratio of negative-sequence voltage increases.

Fig. 5 shows how different values of k_p affect the peak current values of IFC under different phase angles. Because of the periodicity shown in Fig. 4, the difference in phase angle is ranged from 0° to 60°. As shown in Fig. 5, the peak current of IFC reaches its minimum value at $k_p = 0$, as expected from Fig. 2. Moreover, the peak current would decrease if k_p approaches zero, while it would increase if k_p moves away from zero.

III. Design Considerations and Proposed Two-Level Regulation Scheme for Parallel IFCs

A. Design Considerations of Parallel IFCs

In a hybrid ac/dc microgrid with n parallel IFCs between ac and dc buses, one of the converters with the highest power rating is designed as a redundant converter to cancel out parallel IFCs collective active power oscillation. When an unbalanced grid fault occurs, in order to deliver oscillation-free active power to the utility grid, the adjustable current reference coefficients of all IFC are set to $k_p = -1$ (see Fig. 2). However, the unbalanced current of each IFC may exceed its current rating limit, which results in the IFC active power reference reduction. Hence, the total active power transfer capability of the parallel IFCs would be restricted. In order to keep the transferred power of parallel IFCs at constant value during the unbalanced grid fault, k_p of IFCs that their peak currents exceed their currents rating limit move toward zero to decrease the peak currents (see Fig. 5) (although it causes active power oscillation). Then, the k_p of the redundant converter is controlled using (7) to eliminate the active power oscillations of parallel IFCs. Considering (7), k_p of the redundant converter will be less than -1. For this reason, the peak current of the redundant converter will increase (see Fig. 5). Therefore, IFC with higher rating current limitation is considered as redundant IFC. Typical representation of parallel IFCs containing redundant IFC is shown in Fig. 6.

Fig. 7 gives the relationship between the number of converters and the current rating required by the redundant converter under different active power references. In conventional control method ($k_p = -1$ for each converter), maximum output power would be 2910 W if the current rating of the converters is 25 A, shown as blue line in Fig. 7. However, using one redundant converter in the system, more active power can be transferred if redundant converter has higher current rating. For example,

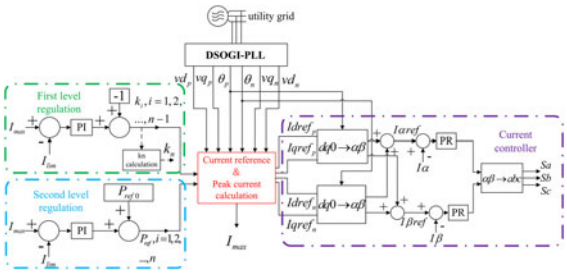

Fig. 8. Block diagram of the proposed two-level control scheme.

maximum active power reference can be as high as 3890 W for each converter if redundant converter has a current rating of 50 A. Here, we assume that only one converter works as redundant converter among IFCs. As the number of converters rises, the current rating of redundant converter also increases linearly. If there are too many converters, more than one converter serves as the redundant converters to decrease their current rating. As an alternative way, to keep the active power transfer capability of parallel IFCs constant, all parallel IFCs can be designed and implemented with high current rating and $k_p = -1$. However, this is not a cost-effective solution as mentioned.

B. Two-level Regulation Scheme for Parallel IFCs

In order to reduce the peak currents of IFCs not to exceed their current rating limits, k_p of common converters should be moved towards zero (peak current reaches its minimum value when $k_p = 0$). However, since the value of peak current varies with the grid fault condition, it is possible that peak currents are still higher than current rating limits when $k_p = 0$. If so, active power references should be reduced for further reduction of common converters' peak currents. In this way, a two-level regulation scheme is desired to restrict peak currents of common converters under all grid fault conditions.

Based on the aforementioned discussion, a two-level regulation scheme for IFCs is proposed. The control scheme block diagram is shown in Fig. 8. As shown in Fig. 8, the first-level regulation determines k_p for each converter and the second-level regulation controls the active power reference $P_{\rm ref}$. It should be noted that k_n of redundant IFC is determined using (7). In the control scheme, $I_{\rm lim}$ and $I_{\rm max}$ represent the current limit and peak current of each IFC, respectively. The detection and sequence separation of utility grid voltage is the key step in the control scheme. Different methods have been investigated up to now, which are mainly using filters and decoupling network [28]–[31]. Recently, a dual second-order generalized integrator (DSOGI-PLL) has been introduced to not only decouple positive- and negative-sequence components but also harmonics in grid voltages [32], [33]. DSOGI-PLL is based on $\alpha\beta$ coordinates, and park transformation is not necessary. As shown in the upper part of Fig. 8, DSOGI-PLL is adopted due to its high accuracy and fast speed response. With the values of k_p, $P_{\rm ref}$, and outputs of DSOGI-PLL, the current reference and the value of peak current can be calculated using (3) and (12) as shown in red block. In the inner current controllers, two PR regulators are used under $\alpha\beta$ coordinates to avoid complex coordination transformation. In Fig. 9, flowchart of the proposed control

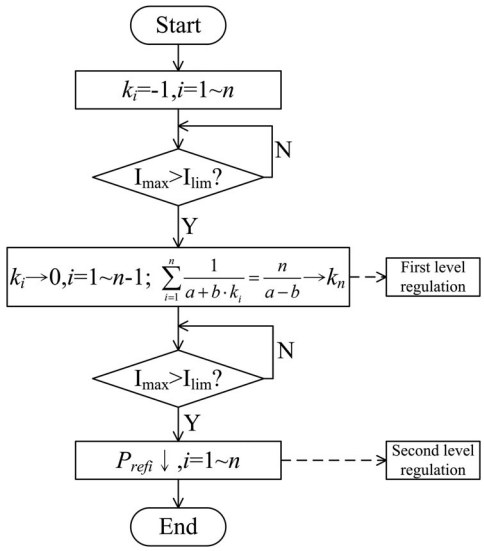

Fig. 9. Flowchart of the proposed control scheme.

scheme is shown. In normal grid conditions, coefficient $k_{\rm p}$ is given as -1 for each converter (namely $k_i = -1,\ i = 1 \sim n$), including common converters and redundant converter. If $I_{\rm max} > I_{\rm lim}$ when grid fault occurs, first-level regulation is activated and k_p of $n-1$ common converters move toward zero. Then, the k_p of the redundant IFC is determined using (7) to cancel out active power oscillations. From analysis on Fig. 5, peak current $I_{\rm max}$ reaches its minimum value when $k_p = 0$ if active power reference does not change. Thus, peak current of common converters reach its minimum value when $k_p = 0$ in first-level regulation. If $I_{\rm max}$ is still larger than $I_{\rm lim}$ after first-level regulation, second-level regulation is activated, and the active power reference $P_{{\rm ref}i},\ i = 1 \sim n$ of IFCs decrease to limit peak currents of all converters further. In summary, first-level regulation limit peak currents of common converters by regulating k_p, while second-level regulation limit peak currents of all converters by decreasing $P_{\rm ref}$.

In this control scheme, the response time is defined as the time interval between the moment when the grid fault occurs and the current reference becomes stable. There are three factors that affect the system's response time. First, the damping factor and PI parameters in DSOGI-PLL are crucial to the performance of voltage components separation [32]. Second, the PI parameters of two-level regulation also influence the response time. Finally, higher band rates for serial communication shorten response time. Here, with suitable parameters, the response time of the control scheme is about two grid-frequency cycles in simulations and experiments.

IV. Simulation Results

In order to verify the proposed control strategy, the parallel operation of two and three IFCs is simulated. The simulation parameters are given in Table I. The voltage fault is a type F fault as described in Section II. As explained in Section II, rated power of redundant converter should be larger than that of common converters. In the simulation, rated power of redundant converter is 4 kW, while those of common converters are 3 kW.

TABLE I
SIMULATION PARAMETERS

DC bus voltage	400 V	*LCL* filter	1.8 mH/4.7 μF/ 1.8 mH
AC bus voltage	110 Vrms/50 Hz	f_s	10 kHz
$I_{\lim}$ (first level)	22 A	I_{lim} (second level)	18 A
Rated power of common converter	3 kW	Rated power of redundant converter	4 kW

A. Tests on Power Complementary Strategy

Three sets of k_A and k_B are tested in three cases: $k_A = k_B = -1$ (Case #1), $k_A = -0.5$, (Case #2), and $k_A = 0$, $k_B = -1.88$ (Case #3). These values of k_A and k_B satisfy the constraint in (7). The active power reference of each IFC is set at 3 kW. The grid fault is type F fault described in [27] which is applied at $t = 1.2\,\mathrm{s}$. The active and reactive power of each IFC and parallel IFCs together with output currents of converter A are shown in Fig. 10.

Except Case #1, the active power of two IFCs is oscillating in Case #2 and Case #3 with the frequency of 100 Hz. It can be seen that active power of two IFCs oscillates in the same amplitude but 180° out of phase. As a result, the output active power of parallel IFCs is constant and free of oscillations. In all three cases, the average reactive power of two IFCs is set on zero. As shown in Fig. 10, the larger k_P results in smaller reactive power oscillation [see (4)]. However, the total reactive power oscillation of parallel IFCs is constant in all three cases, which coincides with the theoretical analysis as shown in (8). From the current waveforms, it is clear that the peak current decreases as k_A moves toward zero. In Case #3, $k_A = 0$ results in balanced three-phase currents and lowest peak current with rated active power reference. From these results, for *n* parallel IFCs, the total active power would be constant if (5) is satisfied and the amplitude of reactive power oscillation will be constant.

Simulations on the parallel operation of three IFCs are given in Fig. 11. Three sets of k_A, k_B, and k_C are tested in three cases: $k_A = k_B = -0.5$, $k_C = -1.915$ (Case #1), $k_A = k_B = 0$, $k_C = -2.667$ (Case #2), and $k_A = 0$, $k_B = -0.5$, $k_C = -2.29$ (Case #3). In Case #1 and Case #2, amplitude of oscillating active power in converters A and B is the same and is half of that in converter C. Amplitude of oscillating active power in Case #3 is all different in three converters. However, total active power is oscillation-free in all three cases. In all cases, the amplitude of parallel IFCs reactive power oscillation is constant although it is different for each converter. It is also observed that amplitude of total reactive power oscillation is 1.5 times larger than that is in Fig. 10 because it is proportional to active power reference and number of IFCs according to (8).

B. Test on the Two-Level Regulation-Based Current Control Scheme

In order to verify the proposed two-level regulation for the active power transfer capability enhancement of parallel IFCs, simulation tests have been conducted. The first-level regulation is tested by setting the current limit of converter A as $I_{\lim} = 22\,\mathrm{A}$, and converter B operates as a redundant converter. Initially, k_A and k_B are set at -1. The control system is activated at $t = 2\,\mathrm{s}$. The top part of Fig. 12 shows simulated waveforms. Before regulation, the peak current of converter A is 26 A and it decreases to 22 A after a short interval, which is also verified by Fig. 5. After regulation, active power of two IFCs begins to oscillate in the same amplitude. Reactive power oscillation of converter A becomes larger than converter B. However, total active power of IFCs is oscillation-free and amplitude of total reactive power oscillation is constant. It can be found that k_A is changed from -1 to -0.44 and k_B is changed from -1 to -1.52 after the regulation. Besides, the system reaches steady state in one cycle after the regulation.

The second-level current control scheme is tested by setting the current limit of converter A at $I_{\lim} = 18\,\mathrm{A}$ and the control system is activated at $t = 2\,\mathrm{s}$. The bottom part of Fig. 12 shows simulated waveforms. The peak current of converter A is limited to 18 A afterward. It is noticeable that output active power remains 6 kW in the interval from 2 to 2.02 s. Actually, first-level regulation is initially activated at $t = 2\,\mathrm{s}$ to decrease the peak current of converter A. However, the peak current could only drops to 19 A with active power reference of 3 kW, which is verified by Fig. 2. Second-level regulation is activated at about $t = 2.02\,\mathrm{s}$ to decrease the peak current further. After regulation, the total active power of parallel IFCs drops from 6 to 5.6 kW, and the reference active power is reduced to $2.8\,\mathrm{kW}$ for each IFC. Besides, amplitude of the total reactive power oscillation becomes a little smaller after regulation. It is because oscillation of reactive power is proportional to active power reference [see (8)]. It can be found that k_A is changed from -1 to 0 and k_B is changed from -1 to -1.88 after the regulation. Fig. 12 also gives current waveforms of converter A. Output currents of converter A becomes symmetrical in three phases because k_A is 0 in steady state. The response time of the system is about two grid-frequency cycles due to that both first- and second-level regulations are activated successively.

Simulation results of the two-level regulation scheme tests on three IFCs are shown in Fig. 13. Converters A and B work as common converters, while converter C works as the redundant one. $I_{\lim}$ is 22 and 18 A for first- and second-level regulation, respectively. In first regulation test, control scheme is activated at $t = 2\,\mathrm{s}$ and active power of all IFCs begins to oscillate. Active power of converters A and B oscillate in the same amplitude, which is half of converter C. Amplitude of total reactive power oscillation is constant after regulation. The second-level regulation is tested on three IFCs. Similar to test on two IFCs, first-level regulation is initially activated and second-level regulation is activated afterward at $t = 2\,\mathrm{s}$. After regulation, the peak currents is limited to $I_{\lim}$.

Although only type F fault caused by two-phase to ground fault is taken as an example to verify the proposed control strategy; this strategy is also feasible under any types of grid fault, including unbalanced and even balanced situations.

V. EXPERIMENTAL RESULTS

The proposed control strategy has been tested on an experimental setup with two parallel IFCs. The schematic and photo

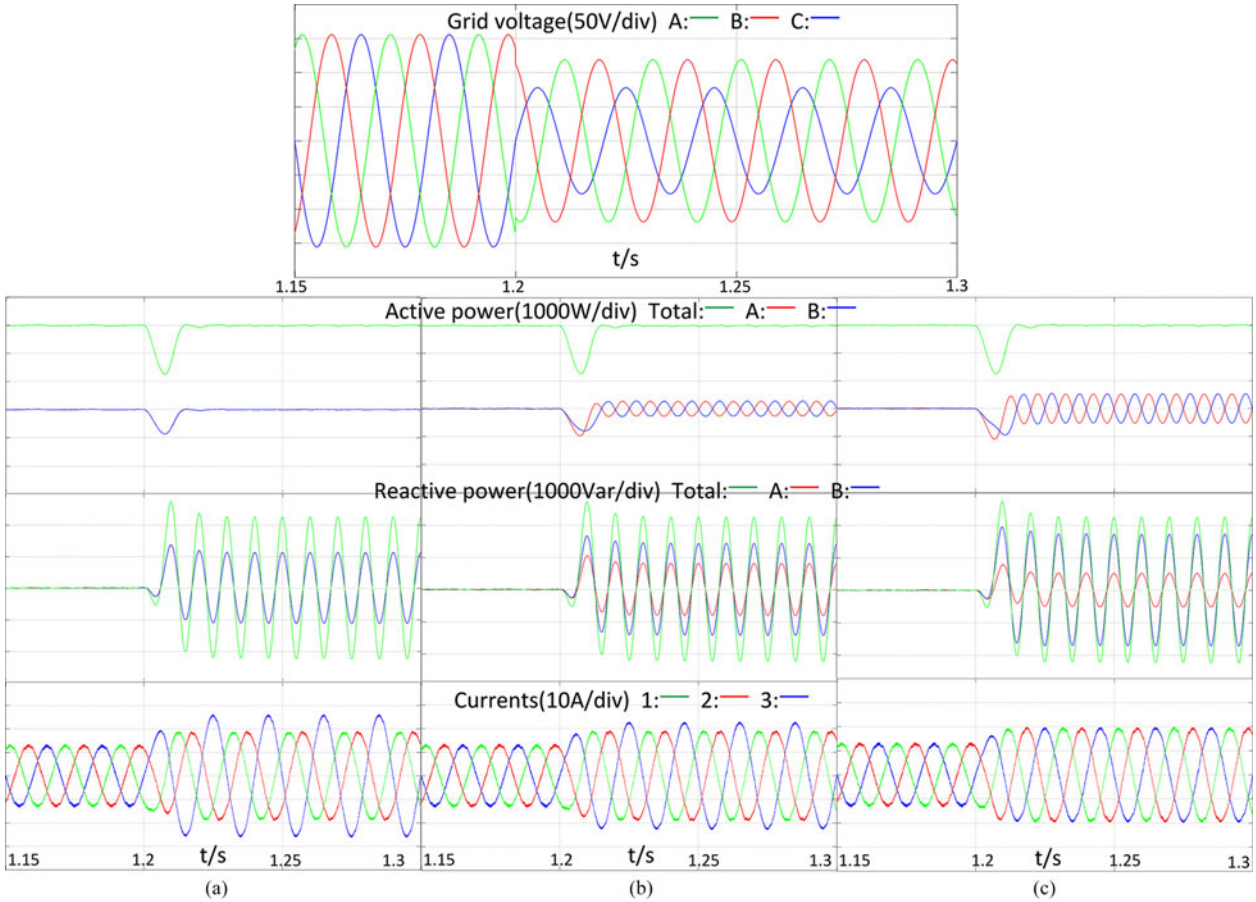

Fig. 10. Simulation results of the power complementary strategy on two parallel IFCs with three sets of k_A and k_B. (a) $k_A = k_B = -1$. (b) $k_A = -0.5$, $k_B = -1.468$. (c) $k_A = 0$, $k_B = -1.88$.

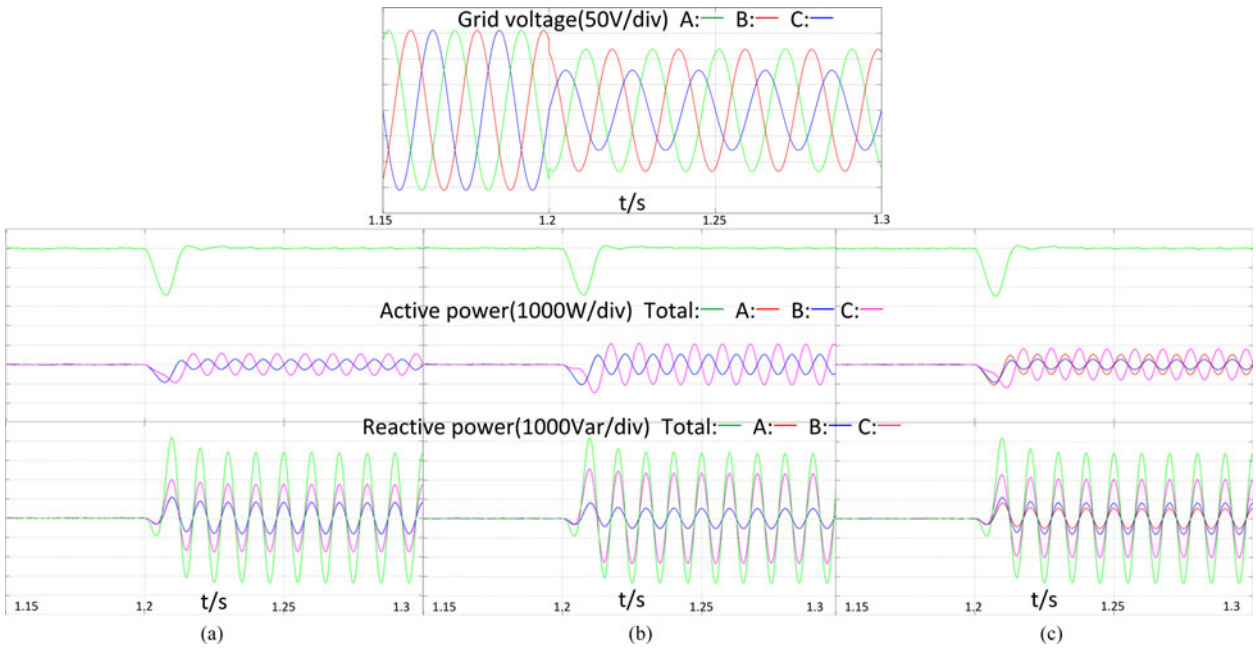

Fig. 11. Simulation results of the power complementary strategy on three parallel IFCs with three sets of k_A, k_B and k_C. (a) $k_A = k_B = -0.5,\ k_C = -1.915$. (b) $k_A = k_B = 0,\ k_C = -2.667$. (c) $k_A = 0$, $k_B = -0.5,\ k_C = -2.29$.

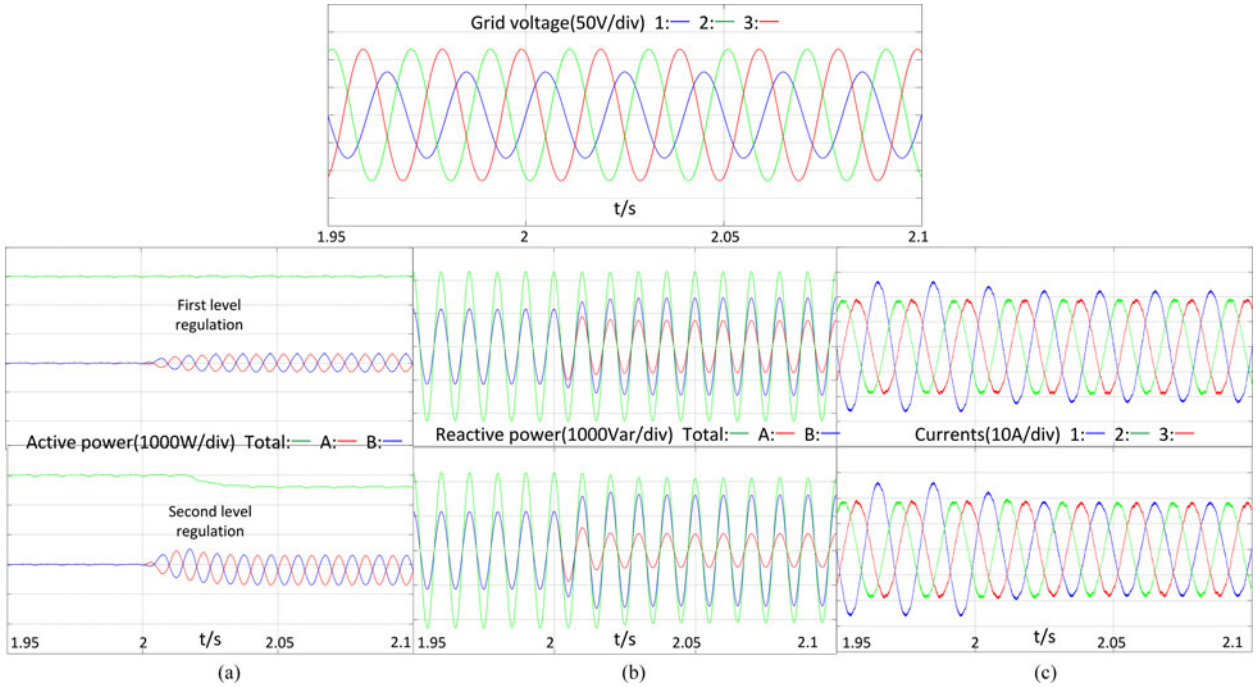

Fig. 12. Simulation results of the two-level regulation scheme tests on two IFCs. (a) Active power. (b) Reactive power. (c) Currents.

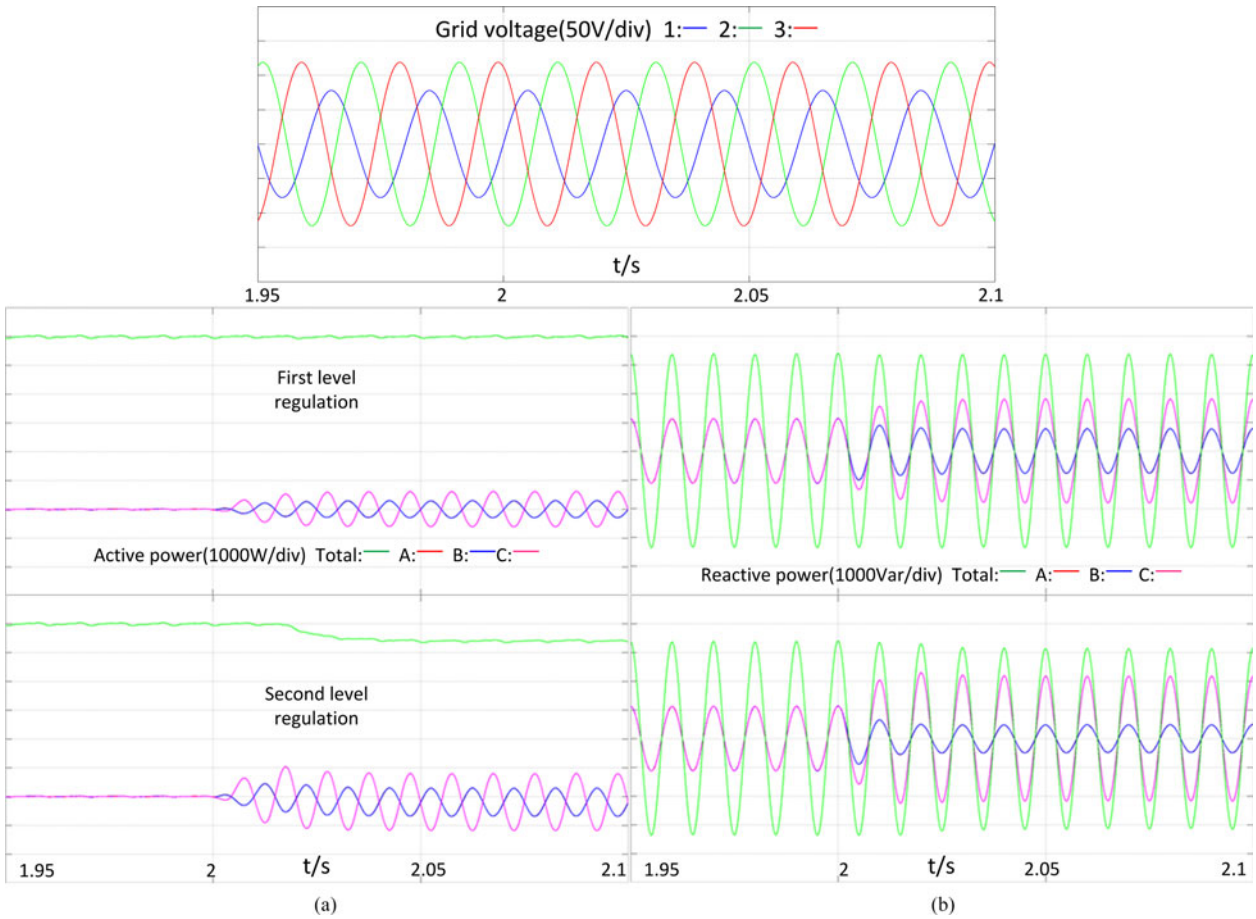

Fig. 13. Simulation results of the two-level regulation scheme tests on three IFCs. (a) Active power. (b) Reactive power.

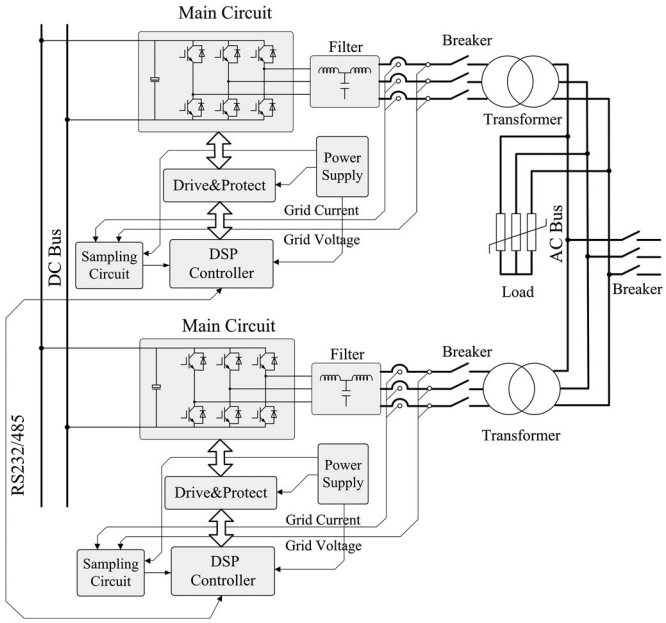

Fig. 14. Schematic of the experimental setup.

Fig. 15. Photo of the experimental setup.

TABLE II
EXPERIMENTAL SPECIFICATIONS

Resistor load	5 Ω/phase	Converter	Myway 5R022
DC source	Chroma 62150H-1000S	AC source	Elgar SW5250
$I_{\lim}$ (first level)	4 A	$I_{\lim}$ (second level)	3 A
Rated active power	650 W/IFC	Voltage fault	Type F

of the experimental setup are shown in Figs. 14 and 15 respectively. The specifications of the experimental setup are listed in Table II and othe parameters are the same as those in simulations. Because the power flow of the ac source is unidirectional, three-phase resistor load is connected between the source and parallel converters to absorb power from both ac source and converters. Besides, the rated active power of the converters is restricted to 650 W because of the limitation of ac source. Since communication is only necessary when the grid fault occurs and during recovery in experiment, a serial communication (RS232/485) is used in this system due to its simplicity to realize and low cost.

A. Test of Power Complementary Strategy Characteristics

Three sets of k_A and k_B are tested in three cases: $k_A = k_B = -1$ (Case #1), $k_A = -0.5,\ k_B = -1.468$ (Case #2), and $k_A = 0,\ k_B = -1.88$ (Case #3). These values of k_A and k_B satisfy the constraint in (7). The steady-state waveforms are shown in Fig. 16. In Case #1, active power of two IFCs is stable and amplitude of reactive power oscillation is the same. In Case #2, active power of two IFCs oscillates with the same amplitude and the two IFCs complement each other. The amplitude of reactive power oscillation of converter A is smaller than converter B in Case #1. However, total reactive power oscillation is the same as in Case #1. In Case #3, active power of two IFCs oscillates with even larger amplitude than Cases #1 and #2, but they still complement each other. The amplitude of reactive power oscillation of converter A is smaller than Case #2. Total reactive power oscillation is the same as Cases #1 and #2. As shown, the peak current of converter A decreases as k_A approaches zero. In Case #3, output currents of converter A become symmetrical in three phases.

B. Test of the Two-level Regulation Scheme

The rated power of the converter 5R022 is 5 kVA and current rating can reach 20 A (peak current). However, rated active power in experiment is set to 650 W because of restrictions of experimental setup mentioned above. To test current restriction of the proposed regulation scheme, here it is assumed that $l_{\lim}$ is the current rating of the converters and it is set in software. In the experiment, converters A and B are defined as the common converter and redundant converter, respectively.

The first-level current control scheme is tested by setting the current rating of converter A to $l_{\lim} = 4$ A, and it is activated at $t = 0.15$ s. The results are shown in the top portion of Fig. 17. As shown, the peak current is limited to 4 A after about 1.5 grid-frequency cycles. After the regulation, the active power of two IFCs starts to oscillate. However, the total active power of parallel IFCs remains oscillation-free. Before $t = 0.15$ s, reactive power oscillations of two IFCs are exactly the same. After regulation, the amplitude of reactive power oscillation of converter A becomes larger and that of converter B becomes smaller, but total reactive power oscillation does not change. The experimental results verify the proposed system performance and simulation results.

Then, second level of the current control scheme is activated at $t = 0.56$ s and the results are shown in the bottom part of Fig. 17. In this test, $l_{\lim}$ is set to 3 A. It should be noticed that the test method used in this experiment is a little different from that used in the simulation. In the simulation, the first and second levels of regulation are activated successively. In the experiment, however, the first level of regulation is already activated at $t = 0.15$ s, so output active power drops immediately at $t = 0.56$ s. Before regulation, the active powers of the two IFCs complement each other and total output active power is 1.3 kW and free of oscillation. After about two grid-frequency

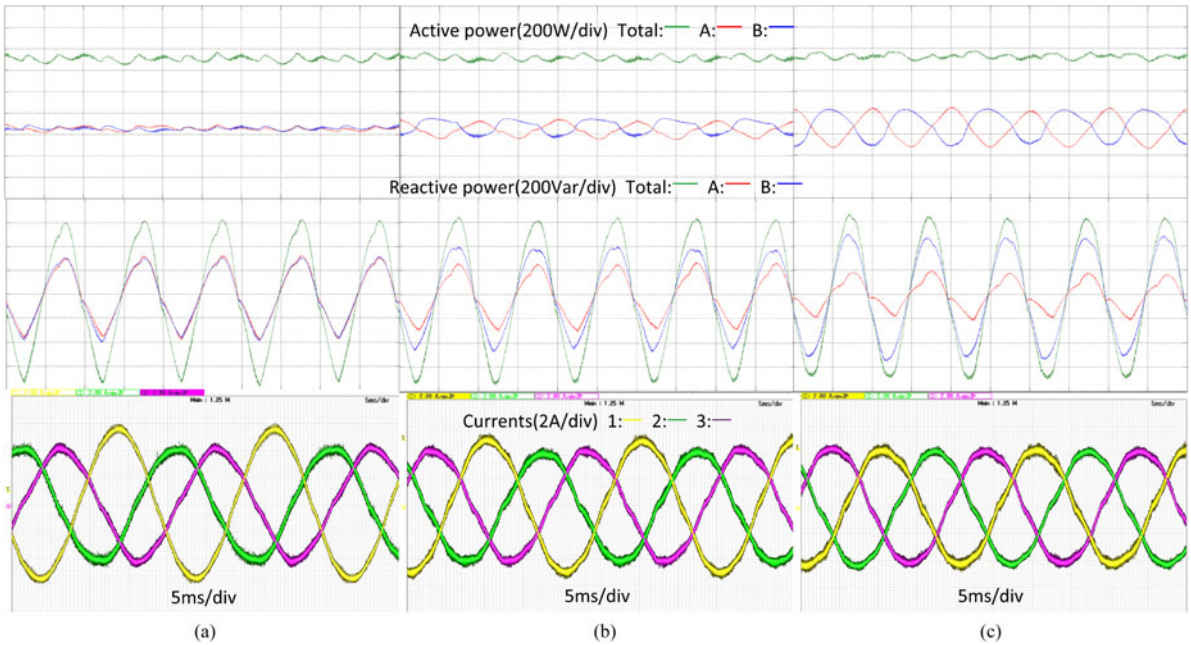

Fig. 16. Experiment results of the power complementary strategy with three sets of k_A and k_B. (a) $k_A = k_B = -1$. (b) $k_A = -0.5$, $k_B = -1.468$. (c) $k_A = 0$, $k_B = -1.88$.

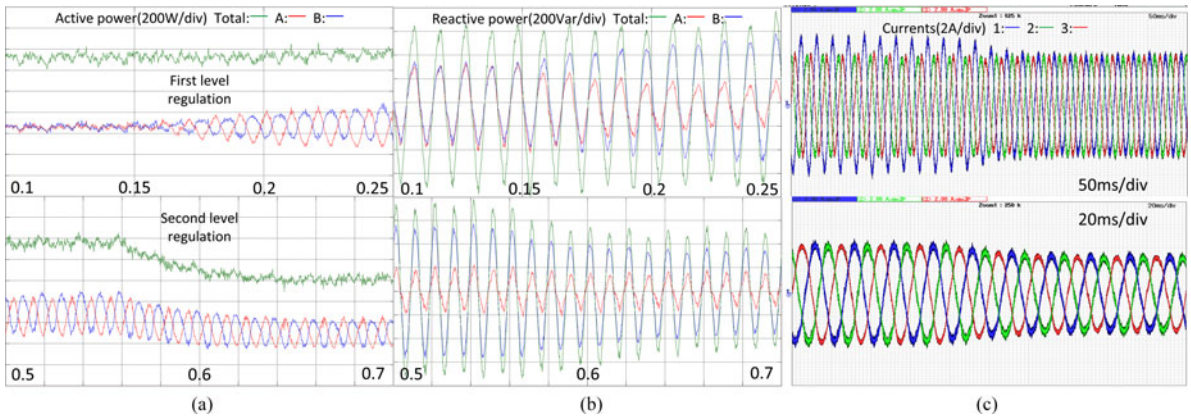

Fig. 17. Experimental results of the two-level regulation scheme tests. (a) Active power. (b) Reactive power. (c) Currents.

cycles, total output active power drops to about 1 kW and is still oscillation-free. The total reactive power oscillation of parallel IFCs decreases a little because of the drop in active power reference Besides, after the second level of regulation, output currents of converter A becomes symmetrical for three phases because k_A changes to zero.

VI. Conclusion

A novel control strategy for parallel operation of IFCs in hybrid ac/dc microgrid under unbalance grid condition is proposed in this paper. By introducing adjustable current references for parallel IFCs, the proposed control strategy enhances the active power transfer capability with zero active power oscillation. In the proposed control strategy, only one IFC serves as a redundant converter with higher current rating to ensure the oscillation-free output active power of parallel IFCs. Simulation and experimental results confirmed the effectiveness of the proposed mechanism and corresponding control scheme. The work in this paper focuses on unity power factor operation of IFCs. Future work will consider reactive power injection from IFCs, and the scenario of all IFCs participated in the active power oscillation cancellation in an optimized manner.

Appendix

A. Total Active Power Derivation

Assuming $\|v^{+2}\| = a$ and $\|v^{-2}\| = b$, we get

$$\begin{aligned}\Delta P_A + \Delta P_B &= P(v^- \cdot v^+) \\ &\quad \times \left(\frac{1+k_A}{\|v^+\|^2 + k_A \|v^-\|^2} + \frac{1+k_B}{\|v^+\|^2 + k_B \|v^-\|^2} \right) \\ &= P(v^- \cdot v^+) \left(\frac{1+k_A}{a + k_A b} + \frac{1+k_B}{a + k_B b} \right). \end{aligned} \tag{A1}$$

Then

$$\begin{aligned} & P(v^- \cdot v^+)\left(\frac{1+k_A}{a+k_Ab}+\frac{1+k_B}{a+k_Bb}\right) \\ = \ & \frac{P(v^- \cdot v^+)}{b}\left(\frac{b+k_Ab}{a+k_Ab}+\frac{b+k_Bb}{a+k_Bb}\right) \\ = \ & \frac{P(v^- \cdot v^+)}{b}\left[\left(1-\frac{a-b}{a+k_Ab}\right)+\left(1-\frac{a-b}{a+k_Bb}\right)\right] \\ = \ & \frac{P(v^- \cdot v^+)}{b}\left[2-(a-b)\left(\frac{1}{a+k_Ab}+\frac{1}{a+k_Bb}\right)\right]. \end{aligned} \tag{A2}$$

From $\Delta P_A + \Delta P_B = 0$, we get

$$\frac{1}{a+b\cdot k_A}+\frac{1}{a+b\cdot k_B}=\frac{2}{a-b}\,. \tag{A3}$$

B. Total Reactive Power Derivation

Assuming $\|v^{+^2}\| = a$ and $\|v^{-^2}\| = b$, reactive power of one single converter is

$$q=\frac{P(1-k_p)(v_\perp^- \cdot v^+)}{\|v^+\|^2+k_p\|v^-\|^2}=\frac{P(1-k_p)(v_\perp^- \cdot v^+)}{a+k_pb}. \tag{A4}$$

Total reactive power of two converters is

$$\begin{aligned} \Delta Q_A+\Delta Q_B = \ & \frac{P(1-k_A)(v_\perp^- \cdot v^+)}{a+k_Ab}+\frac{P(1-k_B)(v_\perp^- \cdot v^+)}{a+k_Bb} \\ = \ & \frac{P(v_\perp^- \cdot v^+)}{b}\frac{(1-k_A)b}{a+k_Ab}+\frac{P(v_\perp^- \cdot v^+)}{b}\frac{(1-k_B)b}{a+k_Bb} \\ = \ & \frac{P(v_\perp^- \cdot v^+)}{b}\left(\frac{a+b}{a+k_Ab}-1\right) \\ & +\frac{P(v_\perp^- \cdot v^+)}{b}\left(\frac{a+b}{a+k_Bb}-1\right) \\ = \ & \frac{P(v_\perp^- \cdot v^+)}{b}\left[(a+b)\left(\frac{1}{a+k_Ab}\right.\right. \\ & \left.\left.+\ \frac{1}{a+k_Bb}\right)-2\right]. \end{aligned} \tag{A5}$$

Substitute (A3) into (A5), yield

$$\begin{aligned} & \Delta Q_A+\Delta Q_B=\tfrac{P(v_\perp^- \cdot v^+)}{b}\left[(a+b)\,\tfrac{2}{a-b}-2\right] \\ & =\tfrac{P(v_\perp^- \cdot v^+)}{b}\,\tfrac{4b}{a-b}=\tfrac{4P(v_\perp^- \cdot v^+)}{a-b}. \end{aligned} \tag{A6}$$

REFERENCES

[1] J. He, Y. W. Li, J. M. Guerrero, F. Blaabjerg, and J. C. Vasquez, "An islanding microgrid power sharing approach using enhanced virtual impedance control scheme," *IEEE Trans. Power Electron.*, vol. 28, no. 11, pp. 5272–5282, Nov. 2013.

[2] T. Ma, B. Serrano, and O. Mohamme, "Distributed control of hybrid AC-DC microgrid with solar energy, energy storage and critical load," in *Proc. Power Syst. Conf.*, Mar. 11–14, 2014, pp. 1–6.

[3] N. Eghtedarpour and E. Farjah, "Power control and management in a hybrid AC/DC microgrid," *IEEE Trans. Smart Grid*, vol. 5, no. 3, pp. 1494–1505, May 2014.

[4] A. P. Martins, A. S. Carvalho, and A. S. Araujo, "Design and implementation of a current controller for the parallel operation of standard UPSs," in *Proc. IEEE Int. Conf. Ind. Electron. Control Instrum.*, Orlando, FL, USA, 1995, pp. 584–589.

[5] J. Rajagopalan, K. Xing, Y. Guo, F. C. Lee, and B. Manners, "Modeling and dynamic analysis of paralleled DC/DC converters with master-slave current sharing control," in *Proc. IEEE Appl. Power Electron. Conf.*, 1996, pp. 678–684.

[6] J. M. Guerrero, J. C. Vasquez, J. Matas, M. Castilla, and L. G. de Vicuna, "Control strategy for flexible microgrid based on parallel line-interactive UPS systems," *IEEE Trans. Ind. Electron.*, vol. 56, no. 3, pp. 726–735, Aug. 2009.

[7] X. Lu, J. M. Guerrero, K. Sun, and J. C. Vasquez, "An improved droop control method for DC microgrids based on low bandwidth communication with DC bus voltage restoration and enhanced current sharing accuracy," *IEEE Trans. Power Electron.*, vol. 29, no. 4, pp. 1800–1812, Apr. 2014.

[8] Y. Li and Y. W. Li, "Power management of inverter interfaced autonomous microgrid based on virtual frequency-voltage frame," *IEEE Trans. Smart Grid*, vol. 2, no. 1, pp. 30–40, Mar. 2011.

[9] X. Liu, P. Wang, and P. C. Loh, "A hybrid AC/DC microgrid and its coordination control," *IEEE Trans. Smart Grid*, vol. 2, no. 2, pp. 278–286, Jun. 2011.

[10] Z. Jiang and X. Yu, "Hybrid DC- and AC-linked microgrids: Towards integration of distributed energy resources," in *Proc. IEEE Energy 2030 Conf.*, 2008, pp. 1–8.

[11] P. C. Loh, D. Li, Y. K. Chai, and F. Blaabjerg, "Autonomous operation of hybrid microgrid with AC and DC subgrids," *IEEE Trans. Power Electron.*, vol. 28, no. 5, pp. 2214–2223, May 2013.

[12] X. Lu, J. M. Guerrero, K. Sun, J. C. Vasquez, R. Teodorescu, and L. Huang, "Hierarchical control of parallel AC-DC converter interfaces for hybrid microgrids," *IEEE Trans. Smart Grid*, vol. 5, no. 2, pp. 683–692, Mar. 2014.

[13] J. Lu, F. Nejabatkhah, Y. W. Li, and B. Wu, "DG control strategies for grid voltage unbalance compensation," in *Proc. IEEE Energy Convers. Congr. Expo.*, 2014, pp. 2932–2939.

[14] S. Iyer, B. Wu, Y. W. Li, and B. N. Singh, "Asymmetrical fault ride-through of three-phase PV systems using four-wire dc-ac converters," in *Proc. IEEE Energy Convers. Congr. Expo. ASIA*, 2014, pp. 3482–3488.

[15] B. Yin, R. Oruganti, S. K. Panda, and A. K. S. Bhat, "An output-power-control strategy for a three-phase PWM rectifier under unbalanced supply conditions," *IEEE Trans. Ind. Electron.*, vol. 55, no. 5, pp. 2140–2151, May 2008.

[16] Y. Suh and T. A. Lipo, "Control scheme in hybrid synchronous stationary frame for PWM AC/DC converter under generalized unbalanced operating conditions," *IEEE Trans. Ind. Appl.*, vol. 42, no. 3, pp. 825–835, May/Jun. 2006.

[17] Z. Li, Y. Li, P. Wang, H. Zhu, C. Liu, and W. Xu, "Control of three-phase boost-type PWM rectifier in stationary frame under unbalanced input voltage," *IEEE Trans. Power Electron.*, vol. 25, no. 10, pp. 2521–2530, Oct. 2010.

[18] F. Wang, H. Mao, D. Xu, and Y. Ruan, "Negative-sequence admittance control scheme for distributed compensation of grid voltage unbalance," in *Proc. Control Model. Power Electron. Conf.*, 2012, pp. 1–8.

[19] A. Camacho, M. Castilla, J. Miret, J. Matas, E. Alarcon-Gallo, L. G. de Vicuna, and P. Marti, "Reactive power control for voltage support during type C voltage-sags," in *Proc. IEEE 38th Annu. Conf. Ind. Electron. Soc.*, 2012, pp. 3462–3467.

[20] A. Camacho, M. Castilla, J. Miret, J. Vasquez, and E. Alarcon-Gallo, "Flexible voltage support control for three-phase distributed generation inverters under grid fault," *IEEE Trans. Ind. Electron.*, vol. 60, no. 4, pp. 1429–1441, Apr. 2013.

[21] M. Castilla, J. Miret, J. L. Sosa, J. Matas, and L. García de Vicuńa, "Grid-fault control scheme for three-phase photovoltaic converters with adjustable power quality characteristics," *IEEE Trans. Power Electron.*, vol. 25, no. 12, pp. 2930–2940, Dec. 2010.

[22] J. Miret, M. Castilla, A. Camacho, L. G. Vicuna, and J. Matas, "Control scheme for photovoltaic three-phase converters to minimize peak currents during unbalanced grid-voltage sags," *IEEE Trans. Power Electron.*, vol. 27, no. 10, pp. 4262–4271, Oct. 2012.

[23] P. Rodriguez, A. V. Timbus, R. Teodorescu, M. Liserre, and F. Blaabjerg, "Flexible active power control of distributed power generation systems during grid faults," *IEEE Trans. Ind. Electron.*, vol. 54, no. 5, pp. 2583–2592, Oct. 2007.

[24] F. Wang, J. L. Duarte, and M. A. M. Hendrix, "Design and analysis of active power control strategies for distributed generation converters under unbalanced grid faults," *IET Gener. Transmiss. Distrib.*, vol. 4, no. 8, pp. 905–916, Aug. 2010.

[25] F. Wang, J. L. Duarte, and M. A. M. Hendrix, "Pliant active and reactive power control for grid-interactive converters under unbalanced voltage dips," *IEEE Trans. Power Electron.*, vol. 26, no. 5, pp. 1511–1521, May 2011.
[26] X. Wang, K. Sun, Y. Li, F. Nejabatkhah, and Y. Mei, "Parallel operation of bi-directional interfacing converters in a hybrid AC/DC microgrid under unbalanced grid conditions," in *Proc. IEEE Energy Convers. Congr. Expo.*, Montreal, QC, Canada, 2015, pp. 4574–4581.
[27] R. Teodorescu, M. Liserre, and P. Rodriguez, "Control of grid converters under grid faults," in *Grid Converters for Photovoltaic and Wind Power Systems*. Hoboken, NJ, USA: IEEE/Wiley, 2011, pp. 237–287.
[28] G. Saccomando and J. Svensson, "Transient operation of grid-connected voltage source converter under unbalanced voltage conditions," in *Proc. IEEE Ind. Appl. Soc. Conf.*, Chicago, IL, USA, 2001, vol. 4, pp. 2419–2424.
[29] H.-S. Song and K. Nam, "Dual current control scheme for PWM converter under unbalanced input voltage conditions," *IEEE Trans. Ind. Electron.*, vol. 46, no. 5, pp. 953–959, Oct. 1999.
[30] M. Reyes, P. Rodriguez, S. Vazquez, A. Luna, R. Teodorescu, and J. M. Carrasco, "Enhanced decouple double synchronous reference frame current controller for unbalanced grid-voltage conditions," *IEEE Trans. Power Electron.*, vol. 27, no. 9, pp. 3934–3943, Sep. 2012.
[31] M. Karimi-Ghartemani and M. R. Iravani, "A method for synchronization of power electronic converters in polluted and variable-frequency environments," *IEEE Trans. Power Syst.*, vol. 19, no. 3, pp. 1263–1270, Aug. 2004.
[32] P. Rodriguez, R. Teodorescu, I. Candela, A. V. Timbus, M. Liserre, and F. Blaabjerg, "New positive-sequence voltage detector for grid synchronization of power converters under faulty grid conditions," in *Proc. Power Electron. Spec. Conf.*, 2006, pp. 1–7.
[33] P. Rodriguez, A. Luna, I. Candela, R. Teodorescu, and F. Blaabjerg, "Grid synchronization of power converters using multiple second order generalized integrators," in *Proc. IEEE 34th Conf. Ind. Electron.*, 2008, pp. 755–760.

Kai Sun (M'12–SM'16) received the B.E., M.E., and Ph.D. degrees in electrical engineering from Tsinghua University, Beijing, China, in 2000, 2002, and 2006, respectively.

He joined the Faculty of Electrical Engineering, Tsinghua University, in 2006, where he is currently an Associate

Professor. From 2009 to 2010, he was a Visiting Scholar of electrical engineering with the Institute of Energy Technology, Aalborg University, Aalborg, Denmark. His current research interests include power electronics for renewable generation systems, microgrids, and active distribution networks.

Dr. Sun is a Member of the IEEE Industrial Electronics Society Renewable Energy Systems Technical Committee, a Member of the IEEE Power Electronics Society Technical Committee of Sustainable Energy Systems, and a Member of Awards Subcommittee of the IEEE Industry Application Society Industrial Drive Committee. He is an Associate Editor for the *Journal of Power Electronics*. He received the Delta Young Scholar Award in 2013.

Xiaosheng Wang (S'13) was born in Xi'an, China, in 1990. He received the B.E. degree in electrical engineering from Tsinghua University, Beijing, China, in 2013, where he is currently working toward the M.E. degree in electrical engineering.

His research interests include modeling and control of distributed generation, renewable energy, and ac/dc microgrid.

Yun Wei Li (S'04–M'05–SM'11) received the B.Sc. degree in electrical engineering from Tianjin University, Tianjin, China, in 2002, and the Ph.D. degree in electrical engineering from Nanyang Technological University, Singapore, in 2006.

In 2005, he was a Visiting Scholar with Aalborg University, Denmark. From 2006 to 2007, he was a Postdoctoral Research Fellow with Ryerson University, Canada. In 2007, he also worked with Rockwell Automation Canada before he joined the University of Alberta, Edmonton, AB, Canada in the same year. Since then, he has been with the University of Alberta, where he is currently a Professor. His research interests include distributed generation, microgrid, renewable energy, high power converters, and electric motor drives.

Dr. Li serves as an Associate Editor for the IEEE TRANSACTIONS ON POWER ELECTRONICS, the IEEE TRANSACTIONS ON INDUSTRIAL ELECTRONICS, the IEEE TRANSACTIONS ON SMART GRID, and the IEEE JOURNAL OF EMERGING AND SELECTED TOPICS IN POWER ELECTRONICS. He received the Richard M. Bass Outstanding Young Power Electronics Engineer Award from the IEEE Power Electronics Society in 2013 and the Second Prize Paper Award of the IEEE TRANSACTIONS ON POWER ELECTRONICS in 2014.

Farzam Nejabatkhah (S'09) received the B.Sc. (Hons.) and M.Sc. (Hons.) degrees in electrical engineering from the University of Tabriz, Tabriz, Iran, in 2009 and 2011, respectively. He is currently working toward the Ph.D. degree at the University of Alberta, Edmonton, AB, Canada.

His research interests include microgrid, power management, power quality, renewable energy and distributed generation, and power converter topologies and control.

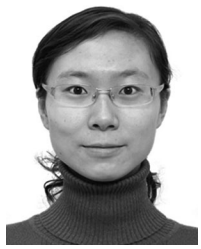

Yang Mei (M'15) received the B.E. degree in electrical engineering from Xi'an Jiaotong University, Xi'an, China, in 2003, and the M.E. and Ph.D. degrees in electrical engineering from Tsinghua University, Beijing, China, in 2005 and 2008, respectively.

She joined the Faculty of North China University of Technology, Beijing, China, in 2008, where she is currently an Associate Professor. From March to August 2010, she was a Visiting Scholar of Electrical Engineering with the Institute of Energy Technology, Aalborg University, Aalborg, Denmark. Her research interests include advanced ac power converters and high performance control of ac motors.

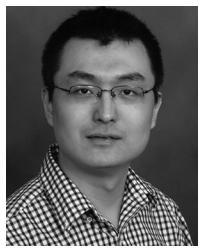

Xiaonan Lu (S'11–M'14) was born in Tianjin, China, in 1985. He received the B.E. and Ph.D. degrees in electrical engineering from Tsinghua University, Beijing, China, in 2008 and 2013, respectively.

From September 2010 to August 2011, he was a Guest Ph.D. Student with the Department of Energy Technology, Aalborg University, Denmark. From October 2013 to December 2014, he was a Postdoctoral Researcher with the Department of Electrical Engineering and Computer Science, University of Tennessee, Knoxville, TN, USA. In January 2015, he joined the Energy Systems Division, Argonne National Laboratory, Lemont, IL, USA, where he is currently a Postdoctoral Appointee. His research interests include modeling and control of power electronic converters in renewable energy systems and microgrids, hardware-in-the-loop real-time simulation, active distribution system, multilevel converters, matrix converters, etc.

Dr. Lu received the Outstanding Reviewer Award for the IEEE TRANSACTIONS ON POWER ELECTRONICS in 2013 and the Outstanding Reviewer Award for the IEEE TRANSACTIONS ON SMART GRID in 2015. He is a Member of the IEEE Power Electronics Society, Industry Applications Society, Industrial Electronics Society, and Power and Energy Society.